



Politecnico di Torino

## Porto Institutional Repository

[Article] Distribution of electrical stimulation current in a planar multilayer anisotropic tissue

*Original Citation:*

Mesin L; Merletti R. (2008). *Distribution of electrical stimulation current in a planar multilayer anisotropic tissue*. In: [IEEE TRANSACTIONS ON BIOMEDICAL ENGINEERING](#), vol. 55 n. 2, pp. 660-670. - ISSN 0018-9294

*Availability:*

This version is available at : <http://porto.polito.it/1865175/> since: December 2008

*Publisher:*

IEEE

*Published version:*

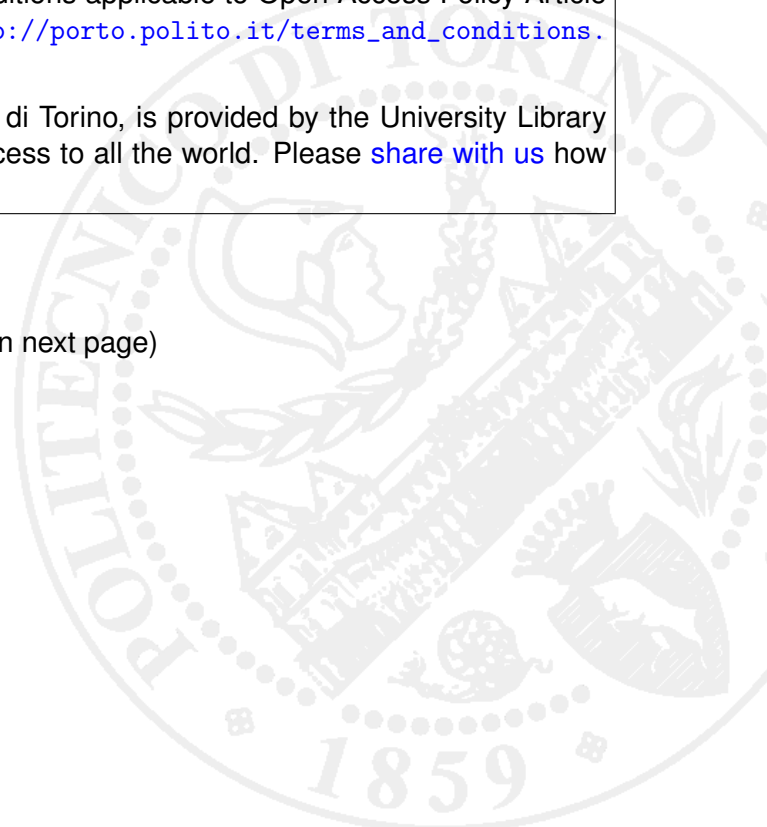
DOI:[10.1109/TBME.2007.902248](https://doi.org/10.1109/TBME.2007.902248)

*Terms of use:*

This article is made available under terms and conditions applicable to Open Access Policy Article ("Public - All rights reserved") , as described at [http://porto.polito.it/terms\\_and\\_conditions.html](http://porto.polito.it/terms_and_conditions.html)

Porto, the institutional repository of the Politecnico di Torino, is provided by the University Library and the IT-Services. The aim is to enable open access to all the world. Please [share with us](#) how this access benefits you. Your story matters.

(Article begins on next page)



# Distribution of Electrical Stimulation Current in a Planar Multi Layer Anisotropic Tissue

Luca Mesin, Roberto Merletti

**Abstract**— This study analytically addresses the problem of neuromuscular electrical stimulation for a planar, multi-layer, anisotropic model of a physiological tissue (referred to as volume conductor). Both conductivity and permittivity of the volume conductor are considered, including dispersive properties. The analytical solution is obtained in the two dimensional Fourier transform domain, transforming in the planes parallel to the volume conductor surface. The model is efficient in terms of computational cost, as the solution is analytical (only numerical Fourier inversion is needed). It provides the current distribution in a physiological tissue induced by an electrical current delivered at the skin surface. Three representative examples of application of the model are considered. 1) The simulation of stimulation artefact during transcutaneous electrical stimulation and EMG detection. Only the effect of the volume conductor is considered, neglecting the other sources of artefact (such as the capacitive coupling between the stimulating and recording electrodes). 2) The simulation of the electrical current distribution within the muscle, and the low pass filter effect of the volume conductor on sinusoidal stimulation currents with different stimulation frequencies. 3) The estimation of the amplitude modulated current distribution within the muscle for interferential stimulation.

The model is devoted to the simulation of neuromuscular stimulation, but the same method could be applied in other fields in which the estimation of the electrical current distribution in a medium induced by the injection of a current from the boundary of the medium is of interest.

**Index Terms**— Electrical stimulation, stimulus artefact, interferential therapy

The authors are with the Laboratorio di Ingegneria del Sistema Neuromuscolare (LISIN), Dipartimento di Elettronica, Politecnico di Torino, Torino, Italy.

Address for correspondence: Luca Mesin, Ph.D., Dipartimento di Elettronica, Politecnico di Torino; Corso Duca degli Abruzzi 24, Torino, 10129 ITALY, Tel. 0039-011-4330476; Fax. 0039-0114330404; e-mail: [luca.mesin@polito.it](mailto:luca.mesin@polito.it)

This work was supported by the European Space Agency Project MESM (Microgravity effects on skeletal muscles investigated by surface EMG and mechanomyogram) contract C15097/01/NL/SH and by a grant from Compagnia di San Paolo.

© 2008 IEEE. Personal use of this material is permitted. Permission from IEEE must be obtained for all other uses, in any current or future media, including reprinting/republishing this material for advertising or promotional purposes, creating new collective works, for resale or redistribution to servers or lists, or reuse of any copyrighted component of this work in other works.

## I. INTRODUCTION

Neuromuscular electrical stimulation generates the contraction of muscle fibres without the central control.

An electrical current is injected from electrodes placed on the skin. It can stimulate the motoneurons, their terminal branches, or the muscle fibres directly. The fibres are activated synchronously, very differently than in the case of voluntary contractions. However, electrical stimulation finds a number of applications in rehabilitation medicine, for the prevention of disuse and denervation atrophy, to improve voluntary control in stroke patients [26], for external control of paralysed muscles (functional electrical stimulation - FES), for reduction of spasticity [27], for muscle training, in fatigue research [2], and to counteract the effects of the permanence in microgravity environments [13].

When a pulse-like current stimulus is provided, the motor units (MU) which are activated generate synchronous action potentials which can be detected at the skin surface (electrically elicited electromyogram - EMG). The potentials add up to form a compound signal, referred to as M-wave. The M-wave provides information on the peripheral properties of the neuromuscular system and on their changes due to fatigue, pathology, exercise, or treatment.

During electrically elicited contractions, the detected surface EMG signal is often perturbed by the stimulation artefact. Stimulation artefact affects the frequency content of the detected signal (giving a high frequency contribution). Furthermore, it biases conduction velocity estimation (as it is a non travelling component). As the artefact perturbs the M-wave of interest, it should be removed. Techniques to reduce the acquired artefact (for example, blanking technique proposed in [10]) and processing methods to remove it (for example, adaptive filter method [15]) were proposed. Furthermore, optimal stimulation current waveforms or surface EMG detection systems were studied ([20][25], but in [14] it was suggested that the selection of a particular stimulation waveform or spatial filter adopted for the M-wave detection have a low effect in reducing artefact, and in [16] it was shown that it is not possible to reduce the artefact without reducing also the M-wave). The choice of an optimal stimulation waveform can also be useful to provide the maximal muscle tension with the minimal stimulation current energy (problem addressed, for example, in [1][17][24]) and, probably, minimal discomfort.

A particular stimulation technique is used in interferential therapy. Two high frequency currents in the range of a few kHz, with a small difference in frequency are used to induce an amplitude modulated current in the excitable tissues [19]. The intent is that of reducing discomfort during stimulation by using a high frequency carrier current penetrating the tissues (exploiting their dielectric property, since current goes through the membrane capacitances without significant ionic shifts) and a low frequency beat current (demodulated by cell membrane non linearity) to elicit action potentials in muscle or nerve fibres.

Electrical stimulation studies can take advantage of mathematical models of stimulation. Stimulation models can support the interpretation of experimental data and give indication for the design of optimal stimulation techniques. By modelling, it is also possible to estimate non accessible quantities (for example the current density distribution inside the muscle). The determination of the potential distribution generated by a system injecting an electrical current from surface electrodes was already addressed in [21], indicating applications in cardiac defibrillation and in electroneurography. Many examples of studies based on finite elements method can be found in the literature for the estimation of the current density distribution in biological tissues. For example, the problem of external defibrillation was addressed in [11]. Analytical solutions can be provided for simple geometries, and for resistive models. As an example, the problem of cardiac stimulation is studied by analytical methods in [29], in the case of spherical symmetry.

Biological tissues have been considered in quasi-stationary conditions in a number of papers on surface EMG simulation during voluntary contractions [4][5]. In such situations, the electric potential in the volume conductor modelling the tissues satisfies Poisson equation [3][9][23]. Nevertheless, permittivity effects can have some importance for surface EMG signals during voluntary contractions [12]. For a plane layer model of the volume conductor such effects can be studied analytically [4].

Dielectric properties of the tissues assume great importance [28] when high frequency components are present in the power spectrum of the stimulation current.

This paper is devoted to the development of an analytical model of electrical stimulation, with the intent of providing a new tool with low computational cost for the investigation of electrical stimulation. In order to obtain an analytical solution, a simple geometry is considered (planar volume conductor), which can give indications only within some approximation. Both conductivity and permittivity effects are considered, including dispersion. Some representative applications to the simulation of stimulation artefact, to the estimation of the current distribution within the muscle for sinusoidal stimulation currents with different frequencies and to interferential stimulation are shown.

## II. METHODS

The electric potential in a volume conductor, considering only the electrical conductivity and neglecting permittivity, is given by the following relationship (Poisson equation) [3][9][23]

$$\nabla \cdot \mathbf{J} = -\nabla \cdot (\underline{\underline{\sigma}} \nabla \varphi) = I \quad (1)$$

where  $\varphi$  is the electric potential (V),  $\mathbf{J}$  the current density in the medium ( $A/m^2$ ),  $I$  the source current density ( $A/m^3$ ), and  $\underline{\underline{\sigma}}$  the conductivity tensor (S/m).

The mathematical model considering also the permittivity of the tissues is the following [28]

$$\nabla \cdot \mathbf{J} = -\nabla \cdot \left[ \left( \underline{\underline{\sigma}} + \varepsilon_0 \varepsilon_r \frac{\partial}{\partial t} \right) \nabla \varphi \right] = I \quad (2)$$

where  $\varepsilon_0 = 8.854 \times 10^{-12}$  F/m is the permittivity of the vacuum and  $\varepsilon_r$  denotes the relative permittivity of the biological tissue considered (which could also be a tensor, as for the anisotropic muscle layer considered in the following). In homogeneous tissues, the condition for neglecting capacitive effects is the following [22][28]

$$\frac{\omega \varepsilon_0 \varepsilon_r}{\sigma} \ll 1 \quad (3)$$

where  $\sigma$  indicates the conductivity of the tissue considered,  $\omega$  is the angular frequency. As the stimulation current can have high frequency content in the power spectrum (it could be a step or an impulsive function), capacitive effects are usually non negligible for a model of electrical stimulation.

Both conductivity and permittivity are frequency dependent in biological tissues [28] causing dispersion. It is simpler to model dispersion in the frequency domain, with respect to the time domain. Transforming Eq. (2) into the frequency domain, and writing explicitly the dependence of conductivity and permittivity on frequency, we have

$$-\nabla \cdot \left[ \left( \underline{\underline{\sigma}}(\omega) + j\omega \varepsilon_0 \varepsilon_r(\omega) \right) \nabla \hat{\varphi} \right] = \hat{I} \quad (2')$$

The equation in the time domain can be obtained by inverse transform. It has an expression more complicated, as it involves a convolution integral [28].

In the following, Eq. (2') is solved for two models of electrical stimulation of a planar volume conductor, relative to two types of electrical conditions: 1) mixed problem, with a portion of the boundary of the volume conductor which is isolated and another which is grounded; 2) isolation of the volume conductor at the skin surface. Two types of material properties were considered, 1) non dispersive and 2) dispersive. To simplify the notation, the dependency of conductivity and permittivity on frequency is not indicated in the following. Nevertheless, all the calculations hold both for non dispersive and for dispersive materials.

### 2.1 Grounded volume conductor

The model of grounded volume conductor is useful to simulate a transcutaneous stimulation set-up, with a small stimulation electrode and a big grounded electrode to close the current path (for example, an adhesive electrode of 1 cm<sup>2</sup> surface placed over a motor point of the biceps muscle and a 40 cm<sup>2</sup>

electrode placed on the triceps muscle [14]). The mathematical model of the stimulation electrode is a point electrode, whereas the grounded electrode is modelled as an infinite plane surface with vanishing potential. For the space invariant volume conductor considered in this paper, the simulation of a stimulation electrode with finite dimensions can be obtained by a convolution integral of the impulse response with the spatial distribution of current injected into the medium (which could be approximated as being uniform on the skin surface under the electrode, neglecting edge effects).

The mathematical problem in the case of a planar volume conductor constituted by one layer (only muscle) insulated at  $y=h$  (for example, the biceps muscle surface) and grounded at  $y=0$  (for example, the triceps muscle surface) is given by adding to Eq. (2) an impulsive Neumann condition at  $y=h$  (i.e., isolation conditions at the surface except for the stimulation point ( $x=0, y=h, z=0$ )) and a homogeneous Dirichlet condition at  $y=0$  (grounding). Transforming by Fourier the  $x, z$  space variables into the spatial frequency variables  $k_x, k_z$  (as in [4]) we obtain the following problem

$$\begin{cases} (\sigma_{MT} + j\omega\varepsilon_0\varepsilon_r^{MT})\partial_{yy}\hat{\phi} - [(\sigma_{MT} + j\omega\varepsilon_0\varepsilon_r^{MT})k_x^2 + (\sigma_{ML} + j\omega\varepsilon_0\varepsilon_r^{ML})k_z^2]\hat{\phi} = 0 & 0 < y < h \\ (\sigma_{MT} + j\omega\varepsilon_0\varepsilon_r^{MT})\partial_y\hat{\phi}|_{y=h} = 1 \\ \hat{\phi}|_{y=0} = 0 \end{cases} \quad (4)$$

where  $\sigma_{MT}, \sigma_{ML}$  are the transversal and longitudinal muscle conductivities, respectively, and  $\varepsilon_r^{MT}, \varepsilon_r^{ML}$  are the transversal and longitudinal muscle permittivities, respectively. The impulsive stimulation current was located in ( $x=0, y=h, z=0$ ), directed downward (i.e., entering the volume conductor). The solution of Eq. (4.I) can be expressed as a sum of exponential functions

$$\hat{\phi}(y; k_x, k_z, \omega) = A(k_x, k_z, \omega)e^{k_{yu}y} + B(k_x, k_z, \omega)e^{-k_{yu}y} \quad (5)$$

where

$$k_{yu} = \sqrt{k_x^2 + \frac{\sigma_{ML} + j\omega\varepsilon_0\varepsilon_r^{ML}}{\sigma_{MT} + j\omega\varepsilon_0\varepsilon_r^{MT}}k_z^2}. \quad (6)$$

Imposing the boundary conditions (4.II) and (4.III), the following analytical solution in the transformed domain is obtained

$$\hat{\phi} = \frac{1}{\sigma_{MT} + j\omega\varepsilon_0\varepsilon_r^{MT}} \frac{\sinh(k_{yu}y)}{k_{yu} \cosh(k_{yu}h)}. \quad (7)$$

The  $\hat{\phi}$  layer solution is interesting because of its simple transfer function. However, even for this simple model, Fourier transform cannot be inverted analytically.

A more realistic model consists in a three layer model: two fat tissue layers ( $L < y < H$  and  $-H < y < -L$ ) and a muscle tissue layer ( $-L < y < L$ ). This model is referred to as *Model 1* (Figure 1a). The mathematical problem in the transformed domain, for an impulse current at ( $x=0, y=H, z=0$ ), and the surface  $y=-H$  grounded, is given by

$$\begin{cases} \partial_{yy}\hat{\phi} - k_y^2\hat{\phi} = 0 & (-H < y < -L) \cup (L < y < H) \\ \partial_{yy}\hat{\phi} - k_{ya}^2\hat{\phi} = 0 & -L < y < L \\ (\sigma_F + j\omega\varepsilon_0\varepsilon_r^F)\partial_y\hat{\phi}|_{y=H} = 1 \\ \hat{\phi}|_{y=L^+} = \hat{\phi}|_{y=L^-} \\ (\sigma_F + j\omega\varepsilon_0\varepsilon_r^F)\partial_y\hat{\phi}|_{y=L^+} = (\sigma_{MT} + j\omega\varepsilon_0\varepsilon_r^{MT})\partial_y\hat{\phi}|_{y=L^-} \\ \hat{\phi}|_{y=-L^+} = \hat{\phi}|_{y=-L^-} \\ (\sigma_F + j\omega\varepsilon_0\varepsilon_r^F)\partial_y\hat{\phi}|_{y=-L^+} = (\sigma_{MT} + j\omega\varepsilon_0\varepsilon_r^{MT})\partial_y\hat{\phi}|_{y=-L^-} \\ \hat{\phi}|_{y=-H} = 0 \end{cases} \quad (8)$$

where  $\sigma_F$  and  $\varepsilon_r^F$  indicate the fat conductivity and permittivity, respectively, and  $k_y = \sqrt{k_x^2 + k_z^2}$ . The solution of Eqs. (8.I) and (8.II) in the three disjoint domains can be expressed as sums of exponential functions

$$\begin{cases} \hat{\phi}_1(y; k_x, k_z, \omega) = A_1(k_x, k_z, \omega)e^{k_y y} + B_1(k_x, k_z, \omega)e^{-k_y y} & L < y < H \\ \hat{\phi}_2(y; k_x, k_z, \omega) = A_2(k_x, k_z, \omega)e^{k_{yu} y} + B_2(k_x, k_z, \omega)e^{-k_{yu} y} & -L < y < L \\ \hat{\phi}_3(y; k_x, k_z, \omega) = A_3(k_x, k_z, \omega)e^{k_y y} + B_3(k_x, k_z, \omega)e^{-k_y y} & -H < y < -L \end{cases} \quad (9)$$

Imposing the 6 conditions (boundary and interface conditions) in Eqs. (8.III)-(8.VIII), the solution is obtained in the transformed domain. The following coefficients define the solution in the muscle layer  $-L < y < L$ , useful to study the current density distribution in the muscle (refer to the Results section and to Figure 2), and the solution in the fat layer in  $L < y < H$ , useful to simulate stimulation artefact (Figure 3)

$$\begin{cases} A_1(k_x, k_z, \omega) = \frac{e^{-Hk_y} (e^{2Lk_y} (e^{4Lk_y} - 1)(k_y^2 \alpha_F^2 - k_{yu}^2 \alpha_M^2) + e^{2Hk_y} (-k_y \alpha_F - k_{yu} \alpha_M)^2 + e^{4Lk_y} (k_y \alpha_F + k_{yu} \alpha_M)^2)}{2k_y \alpha_F (2(e^{4Lk_y} + 1) \cosh[2(H-L)k_y] k_y \alpha_F k_{yu} \alpha_M + (e^{4Lk_y} - 1) \sinh[2(H-L)k_y] (k_y^2 \alpha_F^2 + k_{yu}^2 \alpha_M^2))} \\ B_1(k_x, k_z, \omega) = \frac{e^{-Hk_y} (-4e^{2Lk_y} \cosh[2Lk_y] k_y \alpha_F k_{yu} \alpha_M + (e^{4Lk_y} - 1)(e^{2Hk_y} + e^{2Lk_y}) k_y^2 \alpha_F^2 - (e^{2Hk_y} - e^{2Lk_y}) k_{yu}^2 \alpha_M^2)}{2k_y \alpha_F (2(e^{4Lk_y} + 1) \cosh[2(H-L)k_y] k_y \alpha_F k_{yu} \alpha_M + (e^{4Lk_y} - 1) \sinh[2(H-L)k_y] (k_y^2 \alpha_F^2 + k_{yu}^2 \alpha_M^2))} \\ A_2(k_x, k_z, \omega) = \frac{2e^{Lk_y} (\cosh[(H-L)k_y] k_y \alpha_F + \sinh[(H-L)k_y] k_{yu} \alpha_M)}{-4 \cosh[2(H-L)k_y] \cosh[2Lk_y] k_y \alpha_F k_{yu} \alpha_M - 2 \sinh[2(H-L)k_y] \sinh[2Lk_y] (k_y^2 \alpha_F^2 + k_{yu}^2 \alpha_M^2)} \\ B_2(k_x, k_z, \omega) = \frac{e^{-Lk_y} (-\cosh[(H-L)k_y] k_y \alpha_F + \sinh[(H-L)k_y] k_{yu} \alpha_M)}{2 \cosh[2(H-L)k_y] \cosh[2Lk_y] k_y \alpha_F k_{yu} \alpha_M + \sinh[2(H-L)k_y] \sinh[2Lk_y] (k_y^2 \alpha_F^2 + k_{yu}^2 \alpha_M^2)} \end{cases} \quad (10)$$

where  $\alpha_M = \sigma_{MT} + j\omega\varepsilon_0\varepsilon_r^{MT}$  and  $\alpha_F = \sigma_F + j\omega\varepsilon_0\varepsilon_r^F$ . Similar expressions are obtained for  $A_3$  and  $B_3$  (giving the solution in the grounded fat layer), but are not relevant for our purposes.

## 2.2 Insulated volume conductor

The mathematical problem in the case of a planar volume conductor constituted by one layer (only muscle) insulated at  $y=0$  and infinite for  $y \rightarrow -\infty$  is given by adding to Eq. (2) an impulsive Neumann condition at  $y=0$  (i.e., isolation conditions at the surface except for the stimulation point ( $x=0, y=0, z=0$ )). Transforming by Fourier the  $x, z$  space variables into the spatial frequency variables  $k_x, k_z$  (as in [4]) we obtain the following problem

$$\begin{cases} \partial_{yy}\hat{\phi} - k_{ya}^2\hat{\phi} = 0 & -\infty < y < 0 \\ (\sigma_{MT} + j\omega\varepsilon_0\varepsilon_r^{MT})\partial_y\hat{\phi}|_{y=0} = 1 \end{cases} \quad (11)$$

The solution of Eq. (11.I) is an exponential function

$$\hat{\phi}(y; k_x, k_z, \omega) = A(k_x, k_z, \omega) e^{k_{ya} y} \quad (12)$$

where boundedness for  $y \rightarrow -\infty$  was imposed. Imposing the boundary condition (11.II), the following analytical solution in the transformed domain is obtained

$$\hat{\phi} = \frac{1}{\sigma_{MT} + j\omega\epsilon_0\epsilon_r^{MT}} \frac{e^{k_{ya} y}}{k_{ya}} \quad (13)$$

The one layer solution is interesting because of its simple transfer function, even if Fourier transform cannot be inverted analytically in the case of the considered anisotropic muscle.

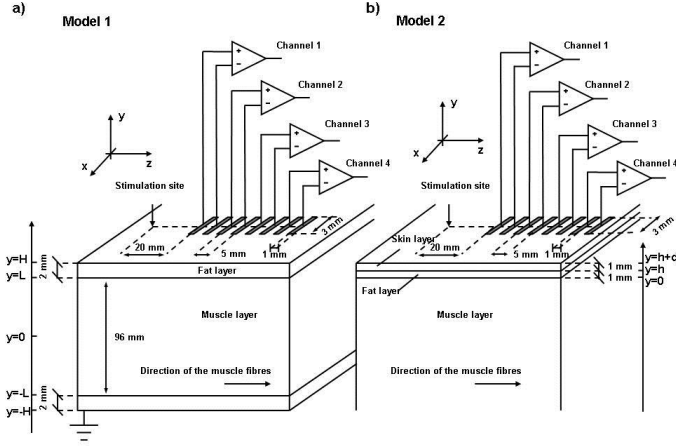


Fig. 1. Representation of the two volume conductors under consideration. a) Model 1 is constituted by three layers, i.e. fat – muscle – fat. The stimulation current is delivered over the first fat surface, the second fat surface is grounded. b) Model 2 is a planar, three layer model, with skin, fat and muscle tissues. The muscle is infinite in the negative y direction. The stimulation current is delivered over the skin surface. Single differential detection channels for surface potential are simulated.

A more realistic model is the three layer volume conductor. Skin and fat layers are considered isotropic, muscle layer is anisotropic. The skin and fat tissues are modelled as infinite planar layers in the x, z directions, bounded in the y direction (skin defined in  $h < y < h + d$ , fat in  $0 < y < h$ ). The muscle is infinite in the x, z directions, semi-infinite in the y direction (defined only in the semi-space  $-\infty < y < 0$ ). This model is referred to as *Model 2* (Figure 1b). Transforming by Fourier the x, z space variables into the spatial frequency variables  $k_x, k_z$  (as in [4]) we obtain the following mathematical problem

$$\begin{cases} \partial_{yy} \hat{\phi} - k_y^2 \hat{\phi} = 0 & h < y < h + d \\ \partial_{yy} \hat{\phi} - k_y^2 \hat{\phi} = 0 & 0 < y < h \\ \partial_{yy} \hat{\phi} - k_y^2 \hat{\phi} = 0 & -\infty < y < 0 \\ (\sigma_s + j\omega\epsilon_0\epsilon_r^S) \partial_y \hat{\phi} \Big|_{y=d} = 1 \\ \hat{\phi} \Big|_{y=h^+} = \hat{\phi} \Big|_{y=h^-} \\ (\sigma_s + j\omega\epsilon_0\epsilon_r^S) \partial_y \hat{\phi} \Big|_{y=h^+} = (\sigma_f + j\omega\epsilon_0\epsilon_r^F) \partial_y \hat{\phi} \Big|_{y=h^-} \\ \hat{\phi} \Big|_{y=0^+} = \hat{\phi} \Big|_{y=0^-} \\ (\sigma_f + j\omega\epsilon_0\epsilon_r^F) \partial_y \hat{\phi} \Big|_{y=0^+} = (\sigma_{MT} + j\omega\epsilon_0\epsilon_r^{MT}) \partial_y \hat{\phi} \Big|_{y=0^-} \end{cases} \quad (14)$$

The solution of Eqs. (14.I), (14.II) and (14.III) in the three disjoint domains can be expressed as sums of exponential functions

$$\begin{cases} \hat{\phi}_1(y; k_x, k_z, \omega) = A_1(k_x, k_z, \omega) e^{k_{1y} y} + B_1(k_x, k_z, \omega) e^{-k_{1y} y} & h < y < h + d \\ \hat{\phi}_2(y; k_x, k_z, \omega) = A_2(k_x, k_z, \omega) e^{k_{2y} y} + B_2(k_x, k_z, \omega) e^{-k_{2y} y} & 0 < y < h \\ \hat{\phi}_3(y; k_x, k_z, \omega) = A_3(k_x, k_z, \omega) e^{k_{3y} y} & -\infty < y < 0 \end{cases} \quad (15)$$

Imposing the 5 conditions (boundary and interface conditions) in Eqs. (14.IV)-(14.VIII) the solution is obtained in the Fourier transform domain. The following coefficients define the solution in the skin layer, useful to simulate stimulation artefact (see the Results section and Figure 3), and the solution in the muscle layer, useful to study the current density distribution in the muscle (Figure 2 and 4) or to simulate interferential therapy (see the Results section and Figure 5)

$$\begin{cases} A_1(k_x, k_z, \omega) = \frac{e^{(d-h)k_1} (-k_1 \alpha_f - k_{1y} \alpha_M) (\alpha_f - \alpha_s) + e^{2hk_1} (k_1 \alpha_f + k_{1y} \alpha_M) (\alpha_f + \alpha_s)}{k_1 \alpha_s (-k_1 \alpha_f + k_{1y} \alpha_M) (\alpha_f + e^{2dk_1} (\alpha_f - \alpha_s) + \alpha_s) + e^{2hk_1} (k_1 \alpha_f + k_{1y} \alpha_M) (\alpha_f + e^{2dk_1} (\alpha_f + \alpha_s) - \alpha_s)} \\ B_1(k_x, k_z, \omega) = \frac{2e^{(d+h)k_1} (k_1 \alpha_f (-\sinh[hk_1] \alpha_f + \cosh[hk_1] \alpha_s) + k_{1y} \alpha_M (-\cosh[hk_1] \alpha_f + \sinh[hk_1] \alpha_s))}{k_1 \alpha_s (-k_1 \alpha_f + k_{1y} \alpha_M) (\alpha_f + e^{2dk_1} (\alpha_f - \alpha_s) + \alpha_s) + e^{2hk_1} (k_1 \alpha_f + k_{1y} \alpha_M) (\alpha_f + e^{2dk_1} (\alpha_f + \alpha_s) - \alpha_s)} \\ A_3(k_x, k_z, \omega) = \frac{4e^{(d+h)k_3} \alpha_f}{(-k_3 \alpha_f + k_{3y} \alpha_M) (\alpha_f + e^{-2dk_3} (\alpha_f - \alpha_s) + \alpha_s) + e^{2hk_3} (k_3 \alpha_f + k_{3y} \alpha_M) (\alpha_f + e^{2dk_3} (\alpha_f + \alpha_s) - \alpha_s)} \end{cases} \quad (16)$$

Similar expressions are obtained for  $A_2$  and  $B_2$  (giving the solution in the fat layer), but are not relevant for our purposes.

### 2.3 Implementation issues

The model was implemented using the software package Matlab (version 6.5).

For a fixed value of y, a three dimensional problem (in the variables x, z, t) was solved for the simulation of the stimulation artefact (Figure 3). A two dimensional problem was solved for a DC stimulation current (Figure 2) or a sinusoidal stimulation current with constant frequency (Figure 4 and 5). The simulation of stimulation artefact requires only the solution at the surface  $y = H$  (for Model 1) or  $y = h + d$  (for Model 2), whereas the simulation of the current density distribution in the muscle requires the solution in the three dimensional muscle layer. Thus, in both cases a three dimensional problem was solved (x, z, t variables for the simulation of stimulation artefact; x, y, z variables for the simulation of the current density distribution).

Time sampling frequency was  $2^{14} = 16384 Hz$ , and 256 samples were considered (which corresponds to a temporal interval of 15.6 ms). The space variables x, z were sampled with step  $\Delta x = 4 mm$ , 64 samples (which corresponds to a square domain with 256 mm side). As a consequence, the

spatial frequencies  $k_x, k_z$  were discretised in the range  $\left[-\frac{\pi}{\Delta x}, \frac{\pi}{\Delta x} - \Delta k\right]$  with sample step  $\Delta k = \frac{2\pi}{64\Delta x}$ . This discretisation allowed low aliasing and tail truncation of the spatial transfer function for each considered value of the time frequency. The analytical solution diverges in  $k_x = 0, k_z = 0$ . The numerical solution in  $k_x = 0, k_z = 0$  was defined by extrapolation (using a best fit cubic extrapolation along the  $k_x$  variable of the four samples before  $k_x = 0$  [exploiting the symmetry property of the solution with respect to  $k_x = 0, k_z = 0$ ]).

After inverting the three dimensional Fourier transform, the resulting solution in the  $x, z, t$  variables at the stimulation surface ( $y = H$  for Model 1,  $y = h + d$  for Model 2) presented small oscillations along the  $x$  and  $z$  axis. The tail truncation of the transfer functions is responsible for such oscillations. To avoid them, the solution for  $x = 0$  and  $z = 0$  was estimated by interpolation (best fit parabolic interpolation considering two samples at each side of the  $x$  and  $z$  axis).

In the case of the simulation of stimulation artefact, the spatial resolution was improved from  $\Delta x = 4 \text{ mm}$  to  $\Delta x = 1 \text{ mm}$  by interpolation (a triangle-based linear interpolation was used; equivalent results were obtained by zero-padding). This interpolation was needed to simulate the detection from a rectangular electrode  $1 \text{ mm} \times 3 \text{ mm}$  (which is the dimension of the detection surface in the linear adhesive array used in [14]). The sum of the potential at the three sample points under the simulated electrode was considered to simulate the potential detected by an electrode, neglecting (as in [4]) the perturbation effect of the electrode on the surrounding potential (the simulation of which would require the solution of a mixed boundary value problem).

### III. RESULTS

The two volume conductors under consideration are shown in Figure 1. Model 1 is constituted by fat and muscle tissues. A fat layer is placed both above the muscle and below. The stimulation current is delivered over the first fat surface, the second fat surface is grounded. Model 2 is a planar, three layer model, with skin, fat and muscle tissues. The muscle is infinite in the negative  $y$  direction. Four single differential detection channels are also shown: they are the channels used for the simulation of stimulus artefact (Figure 3).

Figure 2 shows a comparison between the two considered models. The current density distributions in the muscle in the direction longitudinal (Figure 2a) and transversal (Figure 2b) to the muscle fibres are shown. A DC stimulation current was considered (permittivity effects are absent). The skin conductivity in Model 2 was chosen the same as the fat conductivity, which is the same for the two models:  $\sigma_F = 4 \cdot 10^{-2} \text{ S/m}$ , [7]. The muscle transversal and

longitudinal conductivities were respectively  $\sigma_{MT} = 9 \cdot 10^{-2} \text{ S/m}$ ,  $\sigma_{ML} = 40 \cdot 10^{-2} \text{ S/m}$ , [8] for both models. In this way, the two models are equivalent with the exception that Model 1 has a second fat layer which is grounded. The current density was evaluated by calculating the gradient of the potential in the muscle layer in the Fourier domain and inverting the two dimensional Fourier transform (i.e., from the  $k_x, k_z$  variables to the  $x, z$  variables). For Model 1 we obtain

$$\vec{J} = -\underline{\underline{\sigma}} \nabla \varphi = - \begin{bmatrix} \sigma_{MT} \partial_x \varphi \\ \sigma_{MT} \partial_y \varphi \\ \sigma_{ML} \partial_z \varphi \end{bmatrix} = \mathfrak{Z}^{-2} \begin{pmatrix} jk_x \sigma_{MT} \hat{\varphi}_2(y; k_x, k_z, \omega) \\ -\sigma_{MT} (k_{ya} A_2(k_x, k_z, \omega) e^{k_{ya} y} - k_{yb} B_2(k_x, k_z, \omega) e^{-k_{yb} y}) \\ jk_z \sigma_{ML} \hat{\varphi}_2(y; k_x, k_z, \omega) \end{pmatrix} \quad (17)$$

where  $\hat{\varphi}_2, A_2, B_2$  are given by Eqs. (9.II), (10.III), (10.IV), and  $\mathfrak{Z}^{-2}$  indicates the inversion of the two dimensional Fourier transform. For Model 2, we have

$$\vec{J} = \mathfrak{Z}^{-2} \begin{pmatrix} jk_x \sigma_{MT} \hat{\varphi}_3(y; k_x, k_z, \omega) \\ -\sigma_{MT} k_{ya} A_3(k_x, k_z, \omega) e^{k_{ya} y} \\ jk_z \sigma_{ML} \hat{\varphi}_3(y; k_x, k_z, \omega) \end{pmatrix} \quad (18)$$

where  $\hat{\varphi}_3, A_3$  are given by Eqs. (15.III), (16.III).

The current density amplitude is represented by the length of the vectors shown in Figure 2. Since current density amplitude decays very rapidly, only sample positions close to the stimulation site are shown. The current densities associated to the two different models are very similar close to the stimulation site, and it is not possible to distinguish them. A zoom of the current density is shown inside a square at the bottom left of each picture (the zoom has magnification equal to 60), i.e. close to the surface which is grounded in the first model. It is possible to see that the current density relative to Model 1 is close to be vertical, indicating that the paths of the current density close towards the grounded electrode (as expected). Close to the grounded surface the current densities of the two models differ, but their magnitude is very small (of the order of 1% of the maximum magnitude in the muscle layer).

Level curves are equipotential lines. The levels correspond to the following fractions of the maximum of the potential  $\varphi_M$  in the muscle:  $\frac{\max(\varphi_M)}{2^k}$ ,  $k = 1, \dots, 6$ . The maximum value of  $\varphi_M$

is the same (up to numerical approximation) for both models. Differences in the level curves of the potential become visible at about 10 mm depth in the muscle, where the amplitude of the potential is about one tenth of the maximum value  $\varphi_M$ .

Differences between the potential (and current density) distributions in the longitudinal and transversal sections can be noticed by comparing Figures 2a and 2b, respectively. The distributions in the longitudinal section (Figure 2a) are more extended in the muscle fibre direction ( $z$  direction) with respect to the depth direction ( $y$  direction) because of the anisotropy of muscle conductivity. The distributions in the transversal section (Figure 2b) are constant on circumferences

centred at the stimulation site, due to the isotropy in the sections transversal to the muscle fibre direction.

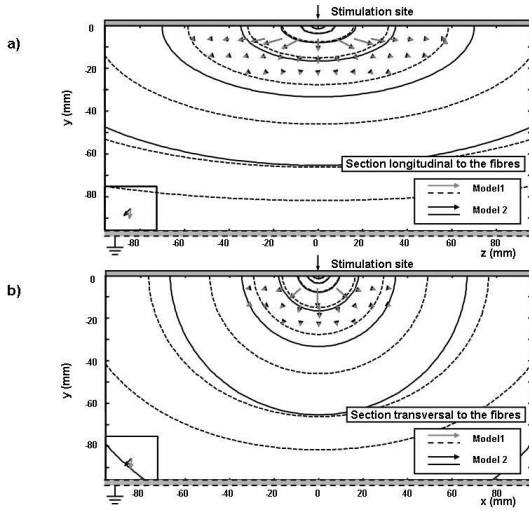


Fig. 2 Current density in the muscle in the direction longitudinal a) and transversal b) to the muscle fibres. DC stimulation current is considered. Skin and fat simulated conductivity  $\sigma_F = 4 \cdot 10^{-2} S/m$ ; muscle transversal and longitudinal conductivities  $\sigma_{MT} = 9 \cdot 10^{-2} S/m$ ,  $\sigma_{ML} = 40 \cdot 10^{-2} S/m$  (the two models are equivalent except for the second fat layer and the grounding of Model 1). Level curves refer to the potential distribution in the muscle  $\varphi_M$  and correspond to  $\frac{\max(\varphi_M)}{2^k}$ ,  $k = 1, \dots, 6$ . A zoom of the current density is shown at the bottom left of each picture (magnification 60), i.e. close to the surface which is grounded in Model 1.

Figure 3 shows an example of application of the model to the simulation of stimulation artefact, for the four single differential channels shown in Figure 1. Stimulation artefact has four sources [18]: 1) the common mode voltage of the limb caused by current flowing through the ground electrode, 2) the voltage gradient due to the current flow through the limb, 3) the capacitive coupling between the stimulating and recording leads, and 4) the band pass filtering characteristics of the recording amplifier. A model of artefact accounting for all of these 4 sources was proposed in [18]. A purely resistive model was considered for the tissues. The model proposed here accounts only for the second source, describing the permittivity effects of the volume conductor, which were neglected in [18]. The patient ground electrode for EMG detection is not simulated, but the contribution of the escape current is negligible if stimulation and detection circuits are isolated. The band pass filter of the recording amplifier can be simulated by filtering the stimulation artefact obtained from the model. The main source which is not taken into account is that related to the capacitive coupling between the stimulating and recording electrodes. To account for this source (which is beyond the aims of this paper), two methods can be applied: 1) the results of the proposed model can be used to build a black box to be inserted in a block diagram of the sources of artefact (as in Figure 7 in [18]), obtaining an approximate simulation of the artefact; 2) the model can be improved by taking into account the capacitive coupling between stimulation and recording electrodes (i.e., solving a mixed boundary value Poisson problem by a numerical method); a more advanced

model would be obtained, but only a numerical solution (to be obtained for example by finite element method) would be available.

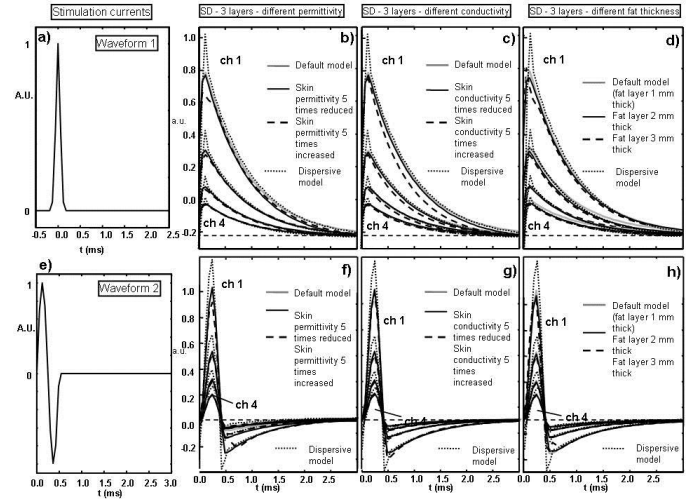


Fig. 3 Example of application of the model to the simulation of stimulation artefacts detected by the four single differential channels shown in Figure 1 (neglecting the capacitive effects of the electrodes). Model 2 is considered. Two stimulation currents are simulated: a) Gaussian (correspondent stimulation artefact in b, c, d), e) sinusoidal stimulation current (correspondent stimulation artefact in f, g, h). Both dispersive and non dispersive materials are considered. Default values for skin, fat, muscle conductivities and permittivities neglecting dispersion are  $\sigma_s = 2.2 \cdot 10^{-2} S/m$ ,  $\epsilon_r^s = 4 \cdot 10^5$ ;  $\sigma_F = 4 \cdot 10^{-2} S/m$ ,  $\epsilon_r^F = 1.5 \cdot 10^5$ ;  $\sigma_{MT} = 9 \cdot 10^{-2} S/m$ ,  $\sigma_{ML} = 40 \cdot 10^{-2} S/m$ ,  $\epsilon_r^{MT} = 4.4 \cdot 10^6$ ,  $\epsilon_r^{ML} = 2 \cdot 10^7$ . The default values are changed by (5 times) increasing or decreasing the permittivity b), f) and the conductivity c), g) of the skin layer, or increasing the fat layer thickness d), h) (from a default value of 1 mm fat thickness to 2 and 3 mm). For dispersive materials, a linear increase of conductivity (300%, 50%, 50% between 0 and 10 kHz for skin, fat and muscle, respectively) and a decrease of permittivity (66% linear decrease between 0 and 10 kHz for the skin, 99% exponential decrease between 0 and 20 kHz for fat and muscle) were assumed.

The stimulation artefact simulated by either Model 1 or Model 2 (using the same parameters) is very similar (results not shown), as the differences between the two models are important only close to the surface which is grounded in Model 1 (see also Figure 2). Thus, Model 2 was used for simulating stimulation artefact, as it allows to consider also the skin layer. In Figure 3 two stimulation waveforms produced by a current stimulator are considered.

1) A Gaussian stimulation current

$$i(t) = \frac{1}{\sqrt{2\pi}w} e^{-\frac{t^2}{2w^2}} \quad (19)$$

is shown in Figure 3a, and the simulated artefact related to such a stimulation current is shown in Figure 3b, 3c, 3d for different values of the parameters. The width  $w$  of the stimulation Gaussian current was  $w = 50 \mu s$ , i.e. high enough to neglect the truncated tails of its Fourier transform (to avoid Gibb's phenomenon, clearly visible for an impulsive stimulation current).

2) A cycle of a sinusoidal function is shown in Figure 3e, and the simulated artefact related to such a stimulation current is shown in Figure 3f, 3g, 3h. Also in this case the support of the

stimulation current was chosen long enough to neglect the truncated tails of its Fourier transform. The stimulator has infinite output impedance at all times.

Both dispersive and non dispersive materials were considered. In the case of non dispersive materials, the following default values for skin, fat, muscle conductivities and permittivities were used:

$$\sigma_S = 2.2 \cdot 10^{-2} S/m, \epsilon_r^S = 4 \cdot 10^5 \quad [30],$$

$\sigma_F = 4 \cdot 10^{-2} S/m, \epsilon_r^F = 1.5 \cdot 10^5 \quad [7], \sigma_{MT} = 9 \cdot 10^{-2} S/m, \sigma_{ML} = 40 \cdot 10^{-2} S/m,$   
 $\epsilon_r^{MT} = 4.4 \cdot 10^6, \epsilon_r^{ML} = 2 \cdot 10^7 \quad [8].$  To assess the effect of changing some of the model parameters, the default values were changed by increasing or decreasing the permittivity (Figure 3b, 3f) and the conductivity (Figure 3c, 3g) of the skin layer by a factor 5, or increasing the fat layer thickness by a factor 3 (Figure 3d, 3h).

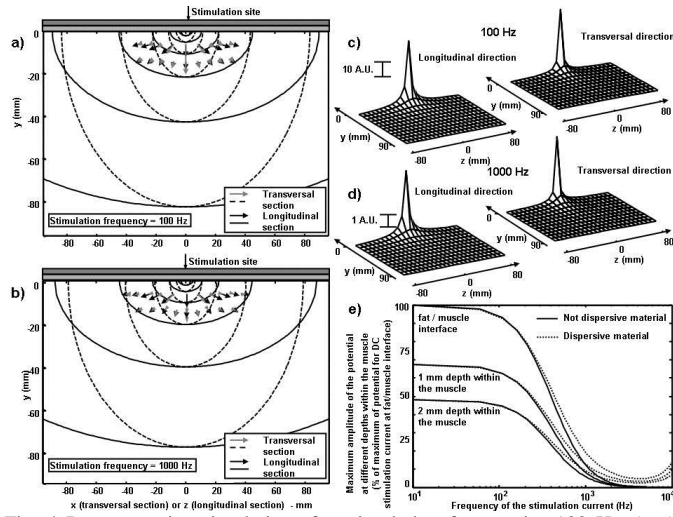


Fig. 4 Representative simulations for stimulation frequencies 100 Hz a), c) and 1000 Hz b), d), with Model 2 with default parameters of non dispersive materials as in Figure 3. Amplitude of the potential (level curves as in Figure 2) and current density in the muscle in the longitudinal and transversal sections with respect to the muscle fibres are shown in a) and b). Three dimensional representation of the amplitudes of the potential (as a function of depth within the muscle and in the directions longitudinal and transversal to the muscle fibres) are shown in c) and d). The maximum amplitudes of the potential at the interface between fat and muscle, at 1 mm depth within the muscle, and at 2 mm depth within the muscle (normalised with respect to the maximum amplitude for DC stimulation at the fat/muscle interface) are shown in e) as a function of the frequency of the stimulation current, for a range of frequency between 10 Hz and 10 kHz.

In the case of dispersive materials, due to the lack of consensus on dielectric data [6], the dependency of conductivity and permittivity of the tissues on frequency was described by simple models, which determine a small variation with respect to the simulated non dispersive materials. The variation of conductivity and permittivity were assumed to be the followings:

- 1) skin conductivity increases linearly 4 times between 0 and 10 kHz, skin permittivity decreases linearly by 66% between 0 and 10 kHz;
- 2) fat conductivity increases linearly by 50% between 0 and 10 kHz, fat permittivity decreases exponentially by 99% between 0 and 20 kHz;
- 3) muscle conductivity increases linearly by 50% between 0 and 10 kHz, muscle permittivity decreases

exponentially by 99% between 0 and 20 kHz (both in longitudinal and transversal direction).

The simulated stimulation artefact has higher amplitude and more rapid variations in the case of dispersive materials, but the decay in time is very similar to the case of non dispersive materials. This is due to the decrease of the permittivity and the increase of the conductivity, which decrease the tissue filtering effect (i.e., the amplitude attenuation) on the high frequency components (refer to Eq. (3)).

Figure 4 shows the current distribution induced in the muscle by sinusoidal stimulation currents of different frequencies. Two representative simulations for two different stimulation frequencies of sinusoidal currents are shown in 4a, 4c (for 100 Hz of stimulation frequency) and in 4b, 4d (1000 Hz). Model 2 with the same default parameters as in Figure 3 was used (both for non dispersive and for dispersive materials). The amplitude of the potential (level curves as in Figure 2) and the current density in the muscle in sections longitudinal and transversal with respect to the muscle fibres are shown in Figure 4a and 4b, for non dispersive material. Three dimensional representations of the amplitudes of the potential in the case of the two frequencies of stimulation considered are shown in Figure 4c and 4d, for non dispersive material. Small differences can be noted in the level curves (as they correspond to relative values with respect to the maximum, as in Figure 2). This indicates that small shape differences affect the amplitude of the potential distribution within the muscle.

The main difference between the potential distributions (and thus also the current distributions) associated to the two simulated stimulation frequencies is the amplitude scale. In the case of stimulation frequency 100 Hz the maximum amplitude is about an order of magnitude bigger than in the case of stimulation frequency 1000 Hz. These differences in the amplitude of the potential within the muscle reflect the effect of permittivity, which is not so important at stimulation frequency 100 Hz, but it is at 1000 Hz (refer to Eq. (3)). The maximum amplitudes of the potential 1) at the interface between fat and muscle, 2) at 1 mm depth within the muscle, and 3) at 2 mm depth within the muscle (normalised with respect to the maximum amplitude for DC stimulation at the fat/muscle interface) are shown in 4e as a function of the frequency of the stimulation current, for a range of frequency between 10 Hz and 10 kHz. Both non dispersive and dispersive materials are considered. The filtering effects of the tissues are equivalent for both materials for low frequencies (up to 2 – 3 kHz). At higher frequencies, the two models of material are quite different: as in dispersive materials permittivity decreases and conductivity increases with frequency, the filtering of high frequency components is lower than for non dispersive materials (in the sense that the attenuation of the amplitude is lower). This result can be interpreted on the basis of the analytical solutions provided in the Method Section. The potential (and hence also the current density) distribution is determined by the 4 functions of frequency  $\frac{\omega\epsilon_0\epsilon_r^S}{\sigma_S}, \frac{\omega\epsilon_0\epsilon_r^F}{\sigma_F}, \frac{\omega\epsilon_0\epsilon_r^{MT}}{\sigma_{MT}}, \frac{\omega\epsilon_0\epsilon_r^{ML}}{\sigma_{ML}}$ . Such functions always increase linearly with frequency for non dispersive materials, whereas for dispersive materials they have a maximum at



about 2-3-kHz and then decrease. By increasing the frequency, when their values approach unity or become lower than unity, the material behaves as in static condition (see Eq. (3)). These results are strongly affected by the parameters and the model of dispersion chosen.

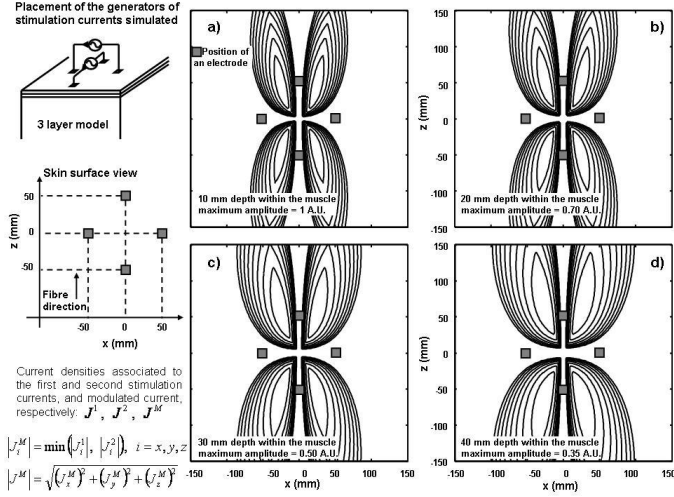


Fig. 5 Example of application of the proposed model (Model 2, with the default parameters as in Figure 3) to interferential stimulation. A sketchy representation of the simulated stimulation set-up and the definition of the beat current are shown on the left. Two stimulation currents with the same amplitude and frequencies 3000 Hz and 3100 Hz (respectively) are simulated. The magnitude of the beat current density is shown for different depths within the muscle in a), b), c) d). Level curves refer to the magnitude of the beat current distribution in the muscle  $J^M$  and correspond to  $\frac{\max(|J^M|)}{1 + 0.5k}$ ,  $k = 1, \dots, 8$ .

An example of application of the proposed model (Model 2, with the default parameters for non dispersive materials as in Figure 3) to interferential stimulation is shown in Figure 5. In interferential stimulation two high frequency sinusoidal currents with a small difference in frequency are used to stimulate excitable tissues. The current field in the volume conductor is the result of two phenomena: 1) an amplitude modulated (beat) current vector having constant direction and 2) a rotating amplitude modulating current vector resulting from the Lissajou combination of the two fields in space. Only the first phenomenon will be considered in this example. In each point of the muscle volume, amplitude modulated current is induced, with beat frequency  $\tilde{f}$  equal to the difference between the stimulation frequencies. The beat current oscillating at low frequency  $\tilde{f}$  is demodulated by the non linear membrane of excitable cells and can induce their activation. The amplitude of the  $i^{\text{th}}$  component of the beat current is equal to the minimum between the  $i^{\text{th}}$  components of the amplitudes induced by the two stimulation currents separately [19]. A sketchy representation of the simulated stimulation set-up and the definition of the beat current are shown in Figure 5 on the left. Two stimulation currents are simulated with the same amplitude and frequencies  $f_1 = 3000$  Hz and  $f_2 = 3100$  Hz, respectively. The magnitude of the beat current density (with beat frequency  $f_2 - f_1 = \tilde{f} = 100$  Hz) is

shown for different depths within the muscle in a), b), c) d). Level curves refer to the magnitude of the beat current distribution in the muscle  $J^M$  and correspond to  $\frac{\max(|J^M|)}{1 + 0.5k}$ ,  $k = 1, \dots, 8$ .

From Figure 5, the beat current vanishes along the x and z axes, i.e. along the lines connecting pairs of stimulation electrodes. Indeed, the two stimulation current vectors (each associated to one of the two stimulators) are orthogonal along those lines (and then beat current vanishes by definition). It is important to observe that, adding current vectors orthogonal in space and with amplitude oscillating at different frequencies generates a rotating current vector, whose amplitude changes periodically (with fundamental frequency  $2\tilde{f}$ ). Such a current is not a beat current, as its direction changes describing a Lissajous curve. Nevertheless, such a current could give a further contribution to the stimulation of excitable membranes. This problem (beyond the aims of this paper) has not been addressed in the literature, yet.

#### IV. DISCUSSION

An analytical method for the simulation of stimulation current distribution within a planar volume conductor is proposed in this paper. The model takes into account the conductivity and permittivity of the tissues, and their possible variation as a function of frequency (dispersive materials). The current distribution is evaluated analytically. The solution method is based on Fourier transforming in the planes parallel to the surface, as in [4].

Two models of the volume conductor are considered, the relative Poisson problems are defined and solved, providing the exact solution in the two dimensional Fourier transform domain. 1) Model 1 is constituted by fat and muscle tissues, with a fat layer placed both above the muscle and below; the stimulation current is delivered over the first fat surface, the second fat surface is grounded. 2) Model 2 is constituted by skin, fat and muscle tissues, with stimulation current delivered over the skin surface and no grounded surface (it is only assumed that the potential vanishes at infinity). The two models are compared and only small differences in the current path within the region of interested muscle can be observed.

Three representative applications of the model are shown. The first is the simulation of stimulation artefact due to the conductivity and dielectric properties of the volume conductor. The capacitive coupling between the stimulation and recording electrodes is not considered. Four single differential detection channels along the muscle fibres are simulated. The exponential tail and the decay of the stimulation artefact for increasing distance from the stimulation site are shown for some representative examples with different simulated anatomies (i.e., for different conductivities, permittivities, tissue thickness, either considering or neglecting dispersion). The simulated artefacts in the case of monopolar Gaussian (or impulsive) stimulation current have a time decay constant of about 1 ms. For both Gaussian and sinusoidal stimulation currents, the amplitude decays about 50% between the first

two single differential channels, 40% between the second couple of channels, 30% between the third couple of channels (10 mm distance between channels, first electrode pair about 20 mm from the stimulation site). The tail is longer and the decay in space is slower in the case in which the signals are low pass filtered by the conditioning system (results not shown). The stimulation artefact is not significantly affected by a fivefold increase or decrease of the conductivity and permittivity of the skin layer or of a threefold increase of the fat thickness is negligible for practical purposes (see Figure 3). Therefore, an accurate estimate of conductivity and permittivity of the skin or fat thickness is not required to simulate the stimulation artefact. The amplitude of the stimulation artefact is affected by dispersion. This is due to the reduced filtering of high frequency components of dispersive materials with respect to non dispersive ones. The tail and decay are the same when either considering or neglecting dispersive properties, as they are related to low frequency components.

A second application of the model is the simulation of the current distribution within the muscle volume, as a function of the simulated anatomy and stimulation current. The decay of the magnitude of the current density in the muscle in sections orthogonal to the skin surface has an exponential shape, with larger decay constant along the direction of muscle fibres. The decay constant in depth is about 10 mm. The simulation of the current distribution within the muscle volume could be useful to estimate the portion of muscle which can be activated by a stimulating current. Considering sinusoidal stimulation currents with different frequencies, the filtering effect of the tissues can be studied. Dispersive materials are similar to non dispersive ones at low frequencies, up to 2-3 kHz. For higher frequencies, dispersive materials determine a lower attenuation of the amplitude of the potential within the muscle with respect to non dispersive materials.

A third example of application is the simulation of interferential stimulation. In interferential stimulation, the physiotherapist can manipulate the amplitudes and the frequencies of two sinusoidal stimulation currents and the location of the electrodes. As the model provides the current distribution in the muscle, it could be a useful tool for the design of optimal stimulation paradigms in interferential therapy. From the shown simulation, some preliminary conclusions can be given. 1) The amplitude of the beat current decreases slowly for increasing depth within the muscle (which confirms that the beat current can penetrate deeply into the muscle tissue). Considering planes of constant depth within the muscle (10, 20, 30 and 40 mm depth), a decrease of about 30% of the amplitude of the beat current was observed for every increase of depth of 10 mm. 2) For the anisotropic model considered, the regions in which the interferential currents have maximum amplitude are in the four quadrants individuated by the two orthogonal lines passing through the positions of the electrodes, with a higher elongation of the distribution of the beat current along the fibre direction.

The analytical approach here proposed has many advantages. 1) The solution is analytical, providing the theoretical dependence of the current distribution on parameters. 2) The

mathematical problem is solved exactly (up to the numerical Fourier inversion), providing a golden standard for numerical methods. 3) The computational cost is low. Nevertheless, the model is quite simple, and this imposes limitations in the applications. However 1) the geometry is planar, and the application of the method to more complex geometries provides only a first order approximation of the actual current distributions; 2) the model does not include structures with complex conductivity, like local inhomogeneities (e.g., glands), blood vessels, bones, muscles with curvilinear fibres. For these cases, a numerical method (as finite elements method) is required.

Although applications in the field of neuromuscular electrical stimulation are discussed, the same simulation method could be applied in other fields in which the estimation of the electrical current distribution in a medium induced by the injection of a current from the boundary is of interest (for example, see [31] for an application in the field of Earth Sciences).

#### REFERENCES

- [1] S.D. Bennie, J.S. Petrofsky, J. Nisperos, M. Tsurudome, M. Laymon, "Toward the optimal waveform for electrical stimulation of human muscle". *Eur J Appl Physiol.* vol. 88(1-2), pp. 13-9, 2002.
- [2] B. Bigland-Ritchie, J.J. Woods, "Changes in muscle contractile properties and neural control during human muscular fatigue", *Muscle Nerve.* vol. 7(9), pp. 691-9. Review. 1984
- [3] J. Clark, R. Plonsey, "The extracellular potential field of the single active nerve fiber in a volume conductor", *Biophys. Journ.*, vol. 8, pp. 842-64, 1968.
- [4] D. Farina, R. Merletti, "A novel approach for precise simulation of the EMG signal detected by surface electrodes", *IEEE Trans. Biomed. Eng.*, vol. 48, pp. 637-646, 2001.
- [5] D. Farina, L. Mesin, S. Martina, "Advances in surface EMG signal simulation with analytical and numerical descriptions of the volume conductor", *Med. Biol. Eng. Comput.*, vol. 42, pp. 467-476, 2004.
- [6] Gabriel C, Gabriel S, Corthout E., "The dielectric properties of biological tissues: I. Literature survey." *Phys Med Biol.* vol. 41(11), pp. 2231-49, 1996. Review.
- [7] S. Gabriel, R.W. Lau, C. Gabriel, "The dielectric properties of biological tissues: II. Measurements in the frequency range 10 Hz to 20 GHz". *Phys Med Biol.* vol. 41(11), pp. 2251-69, 1996.
- [8] F.L. Gielen, W. Wallinga-de Jonge, K.L. Boon, "Electrical conductivity of skeletal muscle tissue: experimental results from different muscles in vivo". *Med. Biol. Eng. Comput.* vol. 22(6), pp. 569-77, 1984.
- [9] A. Heringa, D.F. Stegeman, G.J. Uijen, J.P. de Weerd, "Solution methods of electrical field problems in physiology", *IEEE Trans. Biomed. Eng.*, vol. 29, pp. 34-42, 1982.
- [10] M. Knaflitz, R. Merletti. "Suppression of simulation artefacts from myoelectric-evoked potential recordings". *IEEE Trans Biomed Eng.* vol. 35(9), pp. 758-63, 1988.

- [11] V.T. Krasteva, S.P. Papazov “Estimation of current density distribution under electrodes for external defibrillation”. *Biomed Eng Online*. vol. 16, pp. 1-7, 2002.
- [12] M.M. Lowery, N.S. Stoykov, J.P.A. Dewald, T.A. Kuiken, “Volume Conduction in an Anatomically Based Surface EMG Model”, *IEEE Trans Biomed Eng.*, vol. 51(12), pp. 2138 – 2147, 2004
- [13] W. Mayr, M. Bijak, W. Girsch, C. Hofer, H. Lanmuller, D. Rafolt, M. Rakos, S. Sauermann, C. Schmutterer, G. Schnetz, E. Unger, G. Freilinger, “MYOSTIM-FES to prevent muscle atrophy in microgravity and bed rest: preliminary report”. *Artif. Organs.*, vol. 23(5), pp. 428-31, 1999.
- [14] F. Mandrile, D. Farina, M. Pozzo, R. Merletti. “Stimulation artefact in surface EMG signal: effect of the stimulation waveform, detection system, and current amplitude using hybrid stimulation technique”. *IEEE Trans. Neural. Syst. Rehabil. Eng.* vol. 11(4), pp. 407-15, 2003.
- [15] F. Mandrile, F. Assumma, D. Farina, K. Englehart, P.A. Parker, R. Merletti, “A Novel Adaptive Filtering Approach for Removing Stimulation Artefact from M-waves”, *XV ISEK Congress*, Boston, MA, June 18-21, ISBN 0-87270-136-0, p. 77, 2004.
- [16] Mandrile F., Farina D., Pozzo M., Merletti R., “The Biphasic Waveform Compensation Technique is not Effective for Reducing the Stimulation Artefact in EMG Recordings”, *XV ISEK Congress*, Boston, MA, June 18-21, ISBN 0-87270-136-0, p. 255, 2004.
- [17] R. Merletti, R. Casale, C. Orizio, S. Marcandelli, A. Merlo, P. Ossola, M. Pozzo, A. Rainoldi, “Advances in neuromuscular electrical stimulation techniques. Optimization of countermeasures for microgravity induced muscular deterioration”, *Microgravity and Space Station Utilization*, 2(2-3-4), 235-237, ISSN 0958-5036, 2001.
- [18] K.C. McGill, K.L. Cummins, L.J. Dorfman, B.B. Berlizot, K. Leutkemeyer, D.G. Nishimura, B. Widrow. “On the nature and elimination of stimulus artefact in nerve signals evoked and recorded using surface electrodes”. *IEEE Trans. Biomed. Eng.*, vol. 29(2), pp.129-37, 1982.
- [19] J. Minasidis, “A study to better understand interferential therapy using inhomogeneous finite element model”, Boston University, Senior project final report, 1997.
- [20] J. Nilsson, J. Ravits, M. Hallet, “Stimulus artefact compensation using biphasic stimulation”, *Muscle Nerve*, vol. 11(6), pp. 597-602, 1988.
- [21] T. Oostendorp, A. van Oosterom, “The potential distribution generated by surface electrodes in inhomogeneous volume conductors of arbitrary shape”, *IEEE Trans. Biomed. Eng.*, vol. 38(5), pp. 409-417, 1991.
- [22] R. Plonsey, D.B. Heppner, “Considerations of quasistationarity in electrophysiological systems”, *Bull. Math. Biophys.*, vol. 29, pp. 657-664, 1967.
- [23] R. Plonsey, “Action potential sources and their volume conductor fields”, *IEEE Trans. on Biomed. Eng.*, vol. 56, pp. 601-611, 1977.
- [24] A. Rainoldi, W.K. Durfee, R. Merletti, “Twitch summation with double stimulation”, *Proc. 7th Vienna International Workshop on Functional Electrical Stimulation*, Vienna, September 12-15, pp. 110-113, 2001.
- [25] M. Reichel, M. Bijak, W. Mayr, H. Lanmüller, D. Rafolt, S. Sauermann, E. Unger, and E. Turkof, “Biphasic stimulation: an alternative approach to minimize the stimulus artefact for diagnostic and for control applications”, *Proc. 7th Vienna International Workshop on Functional Electrical Stimulation*, Vienna, pp. 122-125, 2001.
- [26] C.L. Sadowsky. “Electrical stimulation in spinal cord injury”. *NeuroRehabilitation*, vol. 16(3), pp. 165-9, 2001.
- [27] C. Skold, L. Lonn, K. Harms-Ringdahl, C. Hultling, R. Levi, M. Nash, A. Seiger. “Effects of functional electrical stimulation training for six months on body composition and spasticity in motor complete tetraplegic spinal cord-injured individuals”, *J. Rehabil. Med.*, vol. 34(1):25-32, 2002.
- [28] N.S. Stoykov, M.M. Lowery, A. Taflove, T.A. Kuiken, “Frequency- and time-domain FEM models of EMG: capacitive effects and aspects of dispersion”. *IEEE Trans. on Biomed. Eng.*, vol. 49(8), pp. 763 – 772, 2002.
- [29] N.A. Trayanova, B.J. Roth, L.J. Malden. “The response of a spherical heart to a uniform electric field: a bidomain analysis of cardiac stimulation”. *IEEE Trans Biomed Eng.*, vol. 40, pp. 899-908, 1993.
- [30] T. Yamamoto, Y. Yamamoto, “Electrical properties of the epidermal stratum corneum”, *Med. Biol. Eng.*, vol. 14(2), pp. 151-8, 1976.
- [31] Z-X Li, W. Chen J-B Fan, J. Lu, “A novel mathematical modeling of grounding system buried in multilayer Earth”, *IEEE Trans. on Power Delivery*, vol. 21, pp. 1267 – 1272, 2006.